







Visible-near-middle infrared spanning supercontinuum generation in a silicon nitride (Si_3N_4) waveguide

DMITRY MARTYSHKIN,^{1,*}  VLADIMIR FEDOROV,¹  TAYLOR KESTERSON,¹ SERGEY VASILYEV,²  HAIRUN GUO,^{3,5} JUNQIU LIU,³ WENLE WENG,³ KONSTANTIN VODOPYANOV,⁴ TOBIAS J. KIPPENBERG,³ AND SERGEY MIROV^{1,2} 

¹Department of Physics, University of Alabama at Birmingham, 1530 3rd Avenue South, Birmingham AL 35294, USA

²IPG Photonics – Southeast Technology Center, 100 Lucerne Ln., Birmingham, AL 35211, USA

³Swiss Federal Institute of Technology Lausanne, EPFL STI IEL LPQM2, PHD3 355 Station 3, CH1015 Lausanne, Switzerland

⁴CREOL, The College of Optics and Photonics, Univ. of Central Florida, Orlando, FL 32816, USA

⁵Key Laboratory of Specialty Fiber Optics and Optical Access Networks, Shanghai University, Shanghai 200443, China

*dmartych@uab.edu

Abstract: We demonstrate the generation of a supercontinuum spanning more than 1.5 octaves over the 1.2–3.7 μm range in a silicon nitride waveguide using sub-40-fs pulses at 2.35 μm generated by a 75 MHz Kerr-lens mode-locked Cr:ZnS laser.

© 2019 Optical Society of America under the terms of the [OSA Open Access Publishing Agreement](#)

1. Introduction

Recent progress in generation of optical frequency combs based on femtosecond lasers has revolutionized frequency metrology, enabled development of precision optical atomic clocks, helped to resolve the problem of conversion of optical oscillations to the radio frequency domain, and brought many advantages to the ultrafast time-domain spectroscopy in the visible and near-infrared spectral regions. This progress was made possible mainly due to the availability and simplicity of most widely used Ti:sapphire (Ti:S), and, to some extent, Yb and Er-fiber ultrafast laser systems operating in the 600–1700nm wavelength region. However, for ultrafast gas molecular spectroscopy, remote monitoring of explosives, atmospheric sciences, medical applications in the field of early disease diagnosis via exhaled breath analysis, and many other scientific and industrial applications, generation of frequency combs in the middle-infrared spectral region (MIR) of strong molecular absorption bands (2–20 μm) is highly desirable. Our primary objective is the development of an optical-multiple-octave-spanning ultrafast MIR laser sources based on transition metal doped II-VI semiconductor gain media (e.g., $\text{Cr}^{2+}:\text{ZnSe}$, $\text{Cr}^{2+}:\text{ZnS}$). Such laser sources are ideal for generating supercontinuum in waveguides and fibers as well as driving subharmonic optical parametric oscillators and intrapulse difference frequency generators for implementation of compact and efficient optical frequency combs in the important 2–20 μm spectral range.

Polycrystalline chromium doped ZnS and ZnSe are well suited for generation of ultra-short optical pulses in the MIR range. These materials combine superb ultra-fast laser capabilities with high nonlinearity of wide-bandgap zinc-blende semiconductors. Therefore, polycrystalline Cr:ZnS and Cr:ZnSe support all standard regimes of femtosecond (fs) lasers and amplifiers and also enable efficient frequency conversion of ultra-short pulses via $\chi^{(2)}$ and $\chi^{(3)}$ nonlinearities and random phase matching due to optimal microstructure of the gain media [1]. Due to their broad

absorption and emission bands, Cr:ZnS and Cr:ZnSe are often referred to as the “Ti:sapphire of the middle-infrared”. All recent developments in ultrafast Cr-based laser technology are related to Kerr-lens mode-locking in polycrystalline Cr:ZnS and Cr:ZnSe, which was first achieved in 2014 [2]. The most current achievements include 2–3 optical-cycle oscillators with Watt-level average power and MW-level peak power [3,4,5]. Efficient power scaling of ultra-fast MIR oscillators in simple and robust single-pass polycrystalline Cr:ZnS and Cr:ZnSe amplifiers has been demonstrated, resulting in few optical-cycle MIR sources with multi-Watt (multi-MW) average (peak) powers which operate in very broad range of pulse repetition rates [6,7].

Supercontinuum (SC) generation using photonic waveguides is a promising approach for spectral broadening of pulsed coherent sources at low pulse energies and small footprint. SC generation using femtosecond Cr:ZnS laser in As₂S₃-silica double-nanospike waveguide was reported previously [8]. Many materials like stoichiometric Si₃N₄ (SiN) [9,10], AlGaAs [11], silicon on insulators [12], and chalcogenide glasses [13] are appropriate for integrated nonlinear optics. Among them Si₃N₄ holds a unique place due to its high $\chi^{(3)}$ nonlinearity, absence of two photon absorption in the 1550 nm band, ultralow propagation losses [14], space compatibility [15], CMOS compatible fabrication process, and spectral coverage over the visible-middle-infrared range. For this reason Si₃N₄ has been successfully used in microresonator frequency comb generation (micro-combs) [16] as well as low pulse energy supercontinuum generation [9], as well as mid infrared frequency comb generation [10].

The goal of this work is to demonstrate SC generation in Si₃N₄ waveguides pumped by a radiation of Cr:ZnS femtosecond (fs) oscillator to realize a coherent expansion of the pump laser spectrum enabling self-referenced f - $2f$ stabilization of the Cr:ZnS pump source.

2. Experimental results

The fully oxide cladded waveguide core is made of stoichiometric Si₃N₄ deposited via low-pressure chemical vapor deposition (LPCVD) following the photonic Damascene process described in [14,17,18]. The chips were ranged from 5 to 15 mm long, with double inverse taper mode converters at both ends [19]. In particular, MIR operations require large-cross-section waveguides not only for MIR wave confinement but also for the dispersion engineering in the waveguide. We applied conformal deposition of Si₃N₄, which enables a record-large cross section. The waveguide height is up to 2.3 μm , while the width is selected from 1.0-1.6 μm , as shown in Fig. 2. The waveguide length is from 5-15 mm. On both the input and output side of the waveguide, inverse taper section is introduced for increasing the coupling efficiency. The cross section at the taper end is 0.65 μm in the width and ~ 1.7 μm in the height. Figure 1 shows a simulation of a scenario where a 50 fs pulse centered at 2.4 μm with 6 kW peak power is launched into a Si₃N₄ waveguide with 1.3 μm width and 2.3 μm height. The shown output spectrum is obtained after 4.8 mm propagation distance in the waveguide. The dispersive wave around 4.4 μm is generated by its phase matching to the pump pulse (i.e. the zero-valued relative phase constant in the dispersion landscape), and with the group velocity exceeding the pump wave, it behaves analogous to the Cherenkov radiation.

Numerical simulations are based on the nonlinear Schrodinger equation (NLSE), with full dispersion included which corresponds to the waveguide geometry and is calculated via a finite element method. The dispersion is expressed as a relative difference of wave's phase constant compared with the pump wave (assumed as solitons), i.e.:

$\Delta\beta = \beta(\omega) - \beta(\omega_s) - v_g^{-1}(\omega - \omega_s)$, where $\beta(\omega)$ indicates the wave's phase constant (also called propagation constant), ω_s is the angular frequency of the pump wave, and v_g is the group velocity of the pump wave. The Raman effect is ignored and not included in the simulation, since it is weak in Si₃N₄. For ultra-short femtosecond pulses, the self-steepening effect is included in our simulation, which in the frequency domain is termed as a frequency-dependent Kerr nonlinear coefficient, i.e. $\gamma = \omega n_2 / c A_{eff}$, where ω is the angular frequency of the optical wave, n_2 is the

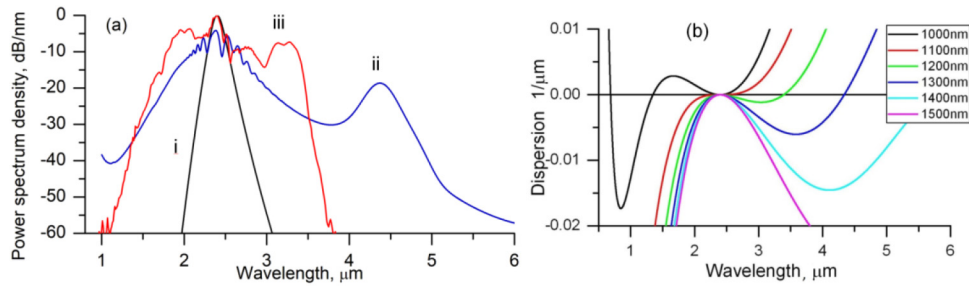


Fig. 1. (a) Simulation of pulse broadening pumped at 2.4 μm wavelength, 50 fs pulse duration, 6 kW peak power. (i) Input spectrum, (ii) Output spectrum for 1.3 μm wide waveguide, (iii) SC spectrum generated in Si₃N₄ waveguide. (b) Dispersion of waveguides with width spanning in 1.0-1.5 μm range.

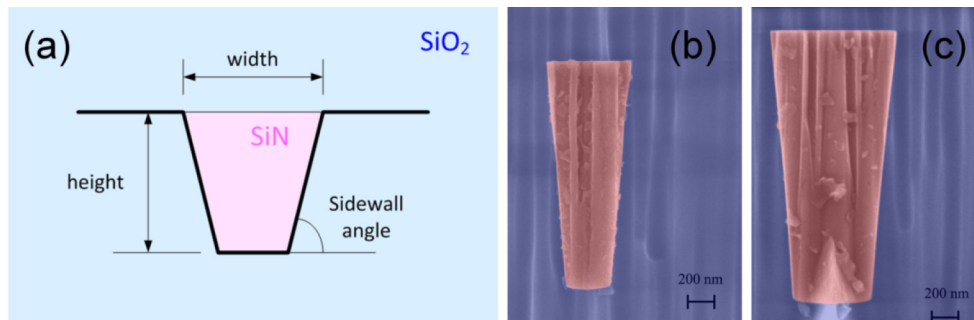


Fig. 2. (a) Schematic representation of Si₃N₄ waveguide (b) SEM image of taper-end cross-section (c) SEM image of waveguide cross-section. Red shaded area indicates the Si₃N₄ and the blue area is the silica cladding.

nonlinear refractive index, A_{eff} indicates the effective mode area, and c is the speed of light in vacuum. We select the waveguide that produces anomalous group velocity dispersion (GVD) at the pumping wavelength, such that the supercontinuum generation is in the soliton regime and is generated by means of the soliton compression over the wave propagation. This process requires short waveguide length (much shorter than the dispersion length $L_D = \tau^2 / |\beta^{(2)}|$, where τ indicates the pumping pulse duration and $\beta^{(2)}$ is the GVD at the pumping wavelength). In the presented Si₃N₄ waveguides and in the presence of the Cr:ZnS laser pulses (pulse duration 45 fs, peak power > 10 kW), the first occurrence of the supercontinuum (also referred to as the first compression point) is typically within few millimeters of the propagation distance. This makes a 5-mm-long waveguide sufficient for the spectral broadening of the pumping laser. Moreover, the soliton regime can ensure a high level of coherence underlying the supercontinuum, since solitons are immune to perturbations, such as power fluctuation and timing jitter, which are typical origins of coherent degradation and can be introduced when operating around the zero GVD.

The pump laser is a CLPF (CLPF-2400-15-80-1-SHG, IPG Photonics) laser system, which is a Kerr-lens mode-locked, middle-infrared laser with the output power up to 1.2 W in fundamental, and 0.3 W in of second harmonic, generated simultaneously in the Cr:ZnS gain element via random quasi-phase-matching process (RQPM) [1]. It operated at 2350 nm with 36 fs pulse duration at 75 MHz repetition rate. Typically, two orthogonal polarizations are generated simultaneously. Figure 3 summarizes the output characteristics of the pump source for horizontal polarization.

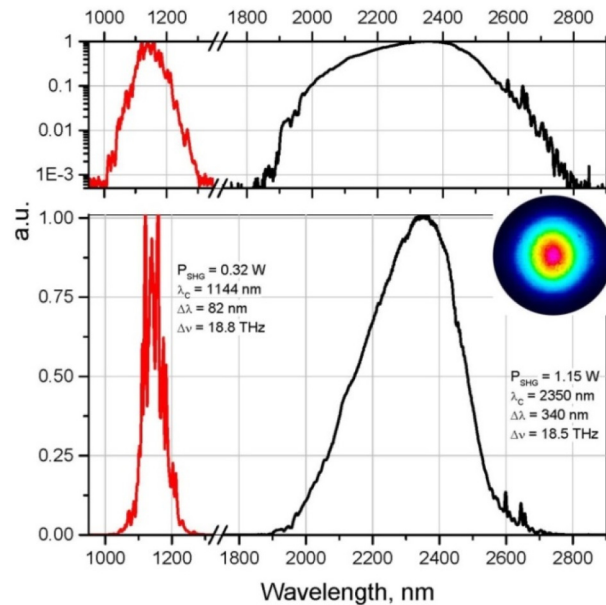


Fig. 3. Spectra of pulses of CLPF laser measured at 5.5 W pump power. Fundamental MIR band of the spectrum is on the right, second harmonic band is on the left. The same spectra are shown in logarithmic (top) and linear (bottom) scales. Numbers near the spectra show measured average power (P), central wavelength (λ_c), and bandwidth ($\Delta\lambda$, $\Delta\nu$ full width at half maximum).

Figure 4 shows the experimental setup for SC generation in Si_3N_4 waveguides. The setup consists of an optical isolator, half wave plate, AR coated molded IR aspheric lens (Black diamond, Thorlabs) placed on a precise XYZ translation stage, gold coated parabolic reflector, monochromator (SpectraPro 300i, Acton Research) and a set of detectors sensitive in VIS, near-IR and MIR spectral regions. We used PMT (P2, Acton Research), TE cooled InGaAs (ID 441, Acton Research), and LN cooled InSb (J10D-M204-R04M-60, EG&G Optoelectronics) for detection of SC spectra. Due to negative GDD of the optical isolator the Cr:ZnS pump laser pulses were stretched to 79 fs and later re-compressed to 45 fs due to the positive GDD of the black diamond lens. The laser beam was focused to a spot of size approximately $5\ \mu\text{m}$ and coupled to the Si_3N_4 waveguide with coupling efficiency of 16-20%. The average power of laser radiation was about 260-300 mW after the optical isolator.

During our experiments, we found that efficiency and SC spectrum strongly depends on geometry of the waveguides as well as polarization of the incident light. The results shown here in Fig. 5 correspond to the best performing waveguide “E7 5 mm W1 #8”. The longer waveguides (e.g 10 and 15 mm) showed worse performance presumably due to losses in SiO_2 cladding. The E7 substrate contains 13 waveguides with width sweeping from 1000 nm to 1600 nm. The 8th waveguide has 1200 nm width with group velocity dispersion minimum at $2.5\ \mu\text{m}$ according to numerical simulations. The incident pump power was 260 mW and had horizontal polarization. The coupling efficiency was about 16%, which corresponds to 0.56 nJ of pulse energy and 12.4 kW peak power. We also have observed that threshold for SC generation was about 50 mW of incident pump power corresponding to 2.4 kW peak pump power. The spectrum of second harmonic, shown in Fig. 4, generated simultaneously in the Cr:ZnS gain element via random quasi-phase-matching process and can be directly used for f - $2f$ stabilization of the Cr:ZnS pump source.

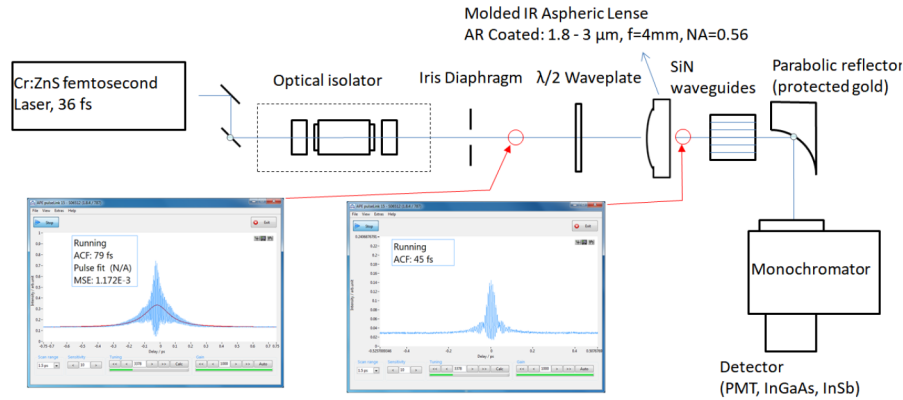


Fig. 4. Experimental set up for SC generation and autocorrelations of Cr:ZnS laser output pulses measured after optical isolator and molded aspheric lens for horizontal polarization.

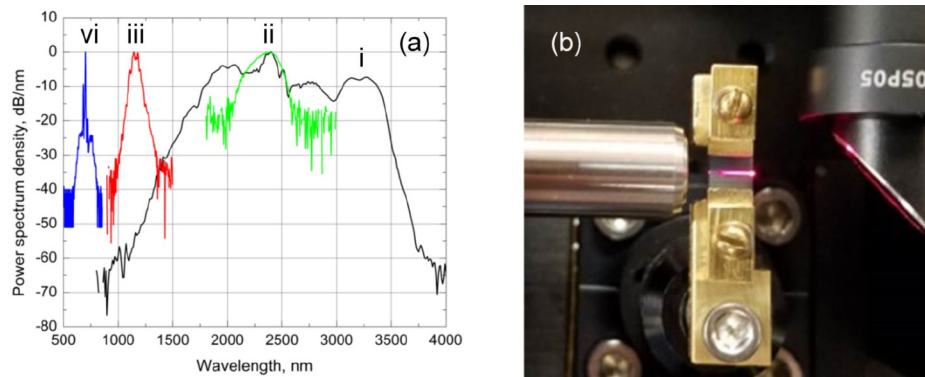


Fig. 5. (a) (i) Supercontinuum spectrum generated in “E7 5 mm W1 #8” waveguide at 260 mW incident average power, 45 fs pulse duration, 75 MHz rate and horizontal polarization (Black); (ii) spectrum of CLPF laser system (Green); (iii) spectrum of near IR second harmonic output of CLPF laser system shown for assessment of possibility of using 2nd harmonic generated in laser gain element and SC for f - $2f$ stabilization of the Cr:ZnS pump source (Red); (vi) Visible emission - the third harmonic generation in Si₃N₄ waveguide (Blue). (b) Picture of the set-up during operation, showing on the left the black diamond lens, at the center Si₃N₄ waveguide shining red, and at the right – gold parabolic reflector.

3. Conclusions

We experimentally demonstrated SC generation spanning over 1.5 octaves over 1.2-3.7 μm spectral range from Si₃N₄ waveguides using 75 MHz Cr:ZnS fs oscillator as a pump. The demonstrated presumably coherent 1.5 octaves spanning bandwidth is ideal for self-referenced f - $2f$ detection of the f_{ceo} . In addition, this represents a promising broadband coherent source for dual comb spectroscopy.

Funding

Defense Advanced Research Projects Agency (DARPA)(HR0011-15-C-005,W31P4Q-15-1-0008 and W31P4Q-16-1-0002).

Acknowledgements

Portions of this work were presented at the “Laser Congress 2018 (ASSL)” in 2018, paper: AW3A.3, doi:ASSL.2018.AW3A.3. The authors acknowledge financial support from Defense Advanced Research Projects Agency (DARPA) through contracts W31P4Q-15-1-0008, W31P4Q-16-1-0002, and HR0011-15-C-0055.

Disclosures

The work reported here partially involves intellectual property developed at the University of Alabama at Birmingham (UAB). This intellectual property has been licensed to the IPG Photonics Corporation. Dr. Fedorov, Dr. Martyshkin and Dr. Mirov declare competing financial interests. Dr. Tobias J. Kippenberg declares competing financial interest as a shareholder of LIGENTEC SA.

References

1. S. Mirov, I. Moskalev, S. Vasilyev, V. Smolski, V. Fedorov, D. Martyshkin, J. Peppers, M. Mirov, A. Dergachev, and V. Gapontsev, “Frontiers of mid-IR lasers based on transition metal doped chalcogenides,” *IEEE J. Sel. Top. Quantum Electron.* **24**(5), 1–29 (2018).
2. S. Vasilyev, M. Mirov, and V. Gapontsev, “Kerr-lens mode-locked femtosecond polycrystalline Cr²⁺:ZnS and Cr²⁺:ZnSe lasers,” *Opt. Express* **22**(5), 5118–5123 (2014).
3. S. Vasilyev, I. Moskalev, M. Mirov, S. Mirov, and V. Gapontsev, “Three optical cycle mid-IR Kerr-lens mode-locked polycrystalline Cr²⁺:ZnS laser,” *Opt. Lett.* **40**(21), 5054–5057 (2015).
4. S. Vasilyev, M. Mirov, and V. Gapontsev, “Mid-IR Kerr-lens mode-locked polycrystalline Cr²⁺:ZnS laser with 0.5 MW peak power,” in *Proc. Adv. Solid-State Lasers*, 2015, Paper AW4A.3.
5. S. Vasilyev, I. Moskalev, M. Mirov, V. Smolski, S. Mirov, and V. Gapontsev, “Kerr-lens mode-locked middle IR polycrystalline Cr:ZnS laser with a repetition rate 1.2 GHz,” in *Proc. Laser Congress 2016 (ASSL, LSC, LAC)*, 2016, Paper AW1A.2.
6. S. Vasilyev, I. Moskalev, M. Mirov, S. Mirov, and V. Gapontsev, “Multiwatt mid-IR femtosecond polycrystalline Cr²⁺:ZnS and Cr²⁺:ZnSe laser amplifiers with the spectrum spanning 2.0–2.6 μm,” *Opt. Express* **24**(2), 1616–1623 (2016).
7. S. Vasilyev, I. Moskalev, M. Mirov, V. Smolski, S. Mirov, and V. Gapontsev, “Ultrafast middle-IR lasers and amplifiers based on polycrystalline Cr:ZnS and Cr:ZnSe,” *Opt. Mater. Express* **7**(7), 2636–2650 (2017).
8. S. Xie, N. Tolstik, J. C. Travers, E. Sorokin, C. Caillaud, J. Troles, P. S. J. Russell, and I. T. Sorokina, “Coherent octave-spanning mid-infrared supercontinuum generated in As₂S₃-silica double-nanospike waveguide pumped by femtosecond Cr:ZnS laser,” *Opt. Express* **24**(11), 12406–12413 (2016).
9. A. R. Johnson, A. S. Mayer, A. Klenner, K. Luke, E. S. Lamb, M. R. E. Lamont, C. Joshi, Y. Okawachi, F. W. Wise, M. Lipson, U. Keller, and A. L. Gaeta, “Octave-spanning coherent supercontinuum generation in a silicon nitride waveguide,” *Opt. Lett.* **40**(21), 5117–5120 (2015).
10. H. Guo, C. Herkommer, A. Billat, D. Grassani, C. Zhang, M. H. P. Pfeiffer, W. Weng, C.-S. Bres, and T. Kippenberg, “Mid-infrared frequency comb via coherent dispersive wave generation in silicon nitride nanophotonic waveguides,” *Nat. Photonics* **12**(6), 330–335 (2018).
11. K. Dolgaleva, W. C. Ng, L. Qian, S. Aitchison, M. C. Camasta, and M. Sorel, “Broadband self-phase modulation, cross-phase modulation, and four-wave mixing in 9-mm-long AlGaAs waveguides,” *Opt. Lett.* **35**(24), 4093–4095 (2010).
12. R. K. W. Lau, M. R. E. Lamont, A. G. Griffin, Y. Okawachi, M. Lipson, and A. L. Gaeta, “Octave-spanning mid-infrared supercontinuum generation in silicon nanowaveguides,” *Opt. Lett.* **39**(15), 4518–4521 (2014).
13. M. R. E. Lamont, B. Luther-Davis, D.-Y. Choi, S. Madden, and B. J. Eggleton, “Supercontinuum generation in dispersion engineered highly nonlinear ($\gamma = 10$ /W/m) As₂S₃ chalcogenide planar waveguide,” *Opt. Express* **16**(19), 14938–14944 (2008).
14. J. Liu, A. S. Raja, M. Karpov, B. Ghadiani, M. Pfeiffer, B. Du, N. J. Engelsen, H. Guo, M. Zervas, and T. J. Kippenberg, “Ultralow-power chip-based soliton micro combs for photonic integration,” *Optica* **5**(10), 1347–1353 (2018).
15. V. Brasch, Q.-F. Chen, S. Schiller, and T. J. Kippenberg, “Radiation hardness of high-Q silicon nitride microresonators for space compatible integrated optics,” *Opt. Express* **22**(25), 30786–30794 (2014).
16. T. J. Kippenberg, A. L. Gaeta, M. Lipson, and M. L. Gorodetsky, “Dissipative Kerr solitons in optical microresonators,” *Science* **361**(6402), eaan8083 (2018).
17. M. P. Pfeiffer, J. Liu, A. S. Raja, T. Morais, B. Ghadiani, and T. Kippenberg, “Ultra-smooth silicon nitride waveguides based on the Damascene reflow process: fabrication and loss origins,” *Optica* **5**(7), 884–892 (2018).

18. M. P. Pfeiffer, C. Herkommer, J. Liu, T. Morais, M. Zervas, M. Geiselmann, and T. Kippenberg, "Photonic Damascene process for low-loss, high-confinement silicon nitride waveguides," *IEEE J. Sel. Top. Quantum Electron.* **24**(4), 1–11 (2018).
19. J. Liu, A.S. Raja, M.H.P. Pfeiffer, C. Herkommer, H. Guo, M. Zervas, M. Geiselmann, and T. Kippenberg, "Double inverse nanotapers for efficient light coupling to integrated photonic devices," arXiv:1803.02662 (2018).